

Langmuir monolayers from functionalized amphiphiles with epoxy terminal groups

Kirsten L. Genson^a, Jason Holzmueller^a, David Vaknin^b, Ovette F. Villavicencio^c,
Dominic V. McGrath^c, Vladimir V. Tsukruk^{a,*}

^aDepartment of Materials Science and Engineering, Iowa State University, Ames, Iowa 50011, USA

^bAmes Laboratory and Department of Physics and Astronomy, Iowa State University, Ames, Iowa 50011, USA

^cDepartment of Chemistry, University of Arizona, P.O. Box 210041, Tuscan, Arizona 85721, USA

Received 1 November 2004; received in revised form 24 March 2005; accepted 8 April 2005

Available online 20 June 2005

Abstract

We studied Langmuir and Langmuir–Blodgett monolayers from amphiphiles with traditional (carboxylic) and bulky functionalized (epoxy) terminal groups at the air–water and air–solid interfaces. We demonstrated that the molecules with a central azobenzene fragment and carboxylic (AA-1 molecule) and bulky epoxy (AE-1 molecule) polar groups formed orthorhombic unit cells with larger than expected area per alkyl tail. The higher order of symmetry indicated by the appearance of higher Q_{xy} peaks revealed that the alkyl tails formed a herringbone structure with limited long range ordering. In the condensed monolayer, the azobenzene group of the AA-1 molecules was oriented vertically in contrast to the AE-1 molecule that was significantly tilted. In addition, the presence of the bulky epoxy focal groups caused a less dense lateral packing of the azobenzene groups. We suggest that the bulky focal group causes intramonolayer packing which can enhance the ability of the chemically grafted azobenzene groups for photoisomerization.

© 2005 Elsevier B.V. All rights reserved.

Keywords: LB films; Surface structures; Atomic force microscopy; X-ray scattering

1. Introduction

Organized surface layers with microstructure and properties influenced by external stimuli are of special interest for many prospective applications [1–4]. Among them, photoresponsive amphiphiles possess the possibility of forming ordered, two-dimensional monolayers with switchable microstructure. Azobenzene molecular fragments have two stable isomers under different wavelength stimulation making these molecules attractive for possible molecular switches and nonlinear optics uses [5,6]. The unique *trans-cis* photoisomerization of the azobenzene molecular fragments is promising for a diverse array of applications, including holographic media [7,8], optical storage [9], reversible optical waveguides [10–12], photoalignment of

liquid crystal systems [13], and drug delivery [14]. The lack of complete control over the molecular orientation and packing structure of the azobenzene fragments within the monolayer hinders their functioning ability. Progress in the control of the orientation and structure of molecules in thin films focuses on both fabrication control and gaining a complete understanding of the interactions between the molecular fragments. Seki and coworkers demonstrated the ability to preserve the photoresponsive behavior of Langmuir–Blodgett (LB) monolayers deposited under certain conditions [15–17]. To realize the ultimate goal of ordered, two-dimensional films with controlled responses to photochromic stimuli in the desired time frame, the molecular structure and packing order of functionalized photochromic amphiphiles must be comprehensively studied at interfaces. Although an efficient photoisomerization reaction was demonstrated for solid monolayers and multilayers, their thermal, temporal, and chemical stability remains, in many

* Corresponding author.

E-mail address: Vladimir@iastate.edu (V.V. Tsukruk).

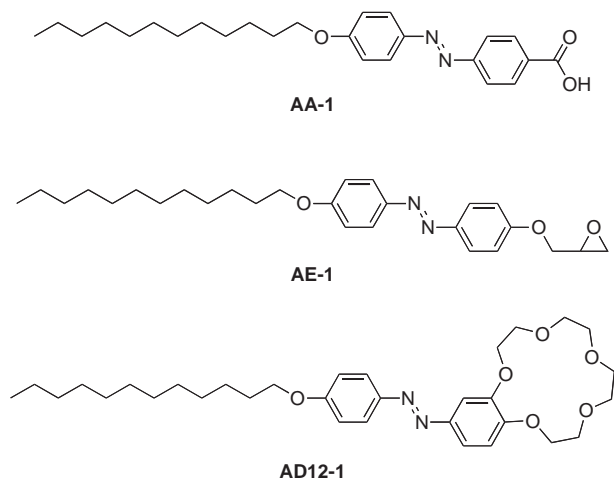


Fig. 1. Structural formulas of molecules AA-1, AE-1, and AD12-1.

cases, questionable. Thus, enhancing the stability of photochromic monolayers in the course of repeatable photoisomerization reorganization by, e.g., chemically grafting them to the solid substrate through appropriate linkers should be considered.

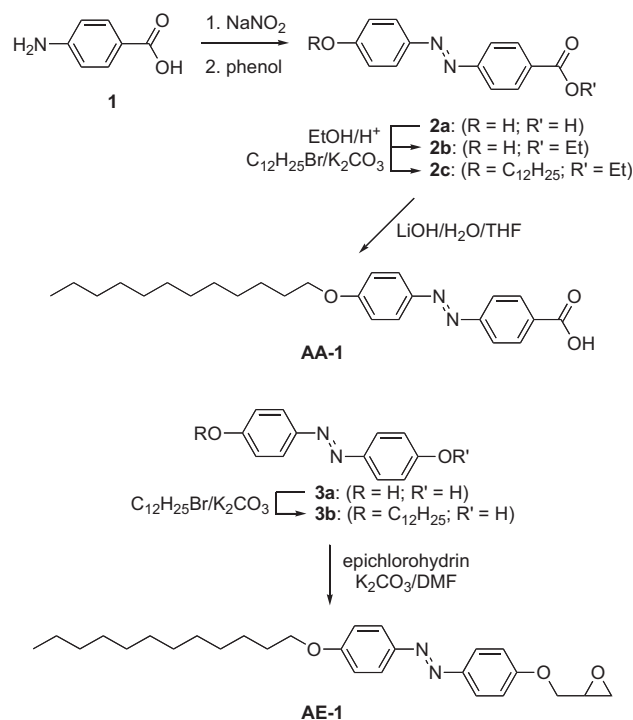
Traditional photochromic amphiphiles with an alkyl tail attached to a compact polar head have been shown to form monolayers with varying degrees of order [13]. Synchrotron-based studies have contributed to the influence of the polar head and the understanding of the packing structures and behaviors of the alkyl chains [18–20]. For example, the inclusion of a spacer group between the polar head and the alkyl tail would control the influence of the terminal group on the molecular interactions as well as complicate the arrangement of the fragments in the packing structure. The focus has progressed from determination of the lattice structure, tilt angle and tilt direction, to the complete understanding of the molecular reorganization [21–23].

In our recent publications, we reported that the attachment of a bulky crown ether polar head to an azobenzene spacer group with an alkyl tail (AD12-1 molecule, Fig. 1) forced the molecules to adopt a “kinked” structure in a densely packed layer at the air–water interface [24,25]. Although the cross-sectional area of the crown ether polar head was calculated to be more than twice the typical 0.20 nm^2 per alkyl tail, the single tail molecule formed a densely packed orthorhombic structure at the air–water interface. The alkyl chains adopted an unusually large tilt angle (58°) to organize in a densely packed layer above the bulky polar head group. We demonstrated that for these molecules efficient photoisomerization can be realized within a condensed monolayer at the air–water interface when sufficient free volume is available for the azobenzene groups to reorganize [26]. The photoisomerization reaction within the monolayer physically deposited on a solid substrate results in structural reorganization, destroying initial local ordering and occasional dewetting of the monolayer [27].

In this paper, we address the effect of the different type of polar head group, including those which are capable of being grafted to a solid substrate, on the azobenzene-containing monolayer packing. We compare the effect of a traditional carboxyl polar head group (AA-1 molecule) versus a larger and functional epoxy polar head group (AE-1 molecule) on monolayer ordering and compared these results with those previously obtained for the crown ether polar head (Fig. 1). We introduce the epoxy head group as a new functional group which facilitates chemical grafting of the photochromic amphiphiles to pre-treated silicon substrates, creating stable, chemically grafted monolayers [28,29]. We observe highly ordered packing structures for these molecules with a “kinked” structure characterized by higher tilt angles of the alkyl tails and loose lateral ordering facilitating the photoisomerization transformation. This study of detailed microstructure of epoxy-terminated amphiphiles is considered as a first step toward fabrication of photochromic LB monolayers chemically stabilized on a solid substrate. The results of a study of their grafting ability and surface behavior, already in progress, will be published elsewhere.

2. Experimental

Compounds AA-1 and AE-1 were prepared by standard synthetic procedures similar to those used before for synthesis of AD12-1 molecules as outlined in Scheme 1. All reagents were purchased from commercial suppliers and used as received unless otherwise indicated. 4-Hydroxyazobenzene (3a) was synthesized according to literature



Scheme 1. Synthesis of compounds.

procedures [30,31]. Nuclear Magnetic Resonance (NMR) spectroscopy was obtained using commercially available instrumentation to confirm chemical composition. Tetrahydrofuran (THF) was distilled under N₂ from sodium-benzophenone ketyl. Dichloromethane (CH₂Cl₂) was distilled under N₂ from CaH₂. Acetone was dried over crushed 3 Å molecular sieves. Flash chromatography was performed by the method of Still et al. [32] using silica gel (40–63 μm, Merck, Darmstadt, Germany). Thin-layer chromatography (TLC) was performed on precoated plates (Silica Gel 60 F₂₅₄, 250 μm, Merck, Darmstadt, Germany).

2.1. 4-(4-Hydroxyphenylazo)benzoic acid (2a)

A solution of NaNO₂ (52.2 g, .766 mol) in a minimal amount of H₂O was added dropwise to a cold (0 °C) solution of *p*-aminobenzoic acid (1) (101 g, 0.733 mol), H₂O (250 mL), and conc. H₂SO₄ (80 mL). The resulting solution was added dropwise to a cold (0 °C) solution of phenol (69.7 g, 0.741 mol) and 2 N NaOH (1900 mL). After stirring for 2 h, the solution was neutralized (5% H₂SO₄), filtered, and dried (MgSO₄). After filtration the filtrate was concentrated to dryness and the resulting solid was dissolved in H₂O and acidified (concentrated H₂SO₄). Benzoic acid 2a (108 g, 58%) was collected as an orange solid by vacuum filtration: mp >250 °C; (literature data [33]: 276 °C). ¹H NMR (250 MHz, *d*₆-acetone) δ 8.22 and 7.93 (AA'BB' pattern, *J*=8.5 Hz, 4H), 7.96 and 7.06 (AA'BB' pattern, *J*=8.9 Hz, 4H).

2.2. Ethyl 4-(4-hydroxyphenylazo)benzoate (2b)

A mixture of 2a (22.6 g, 93.2 mmol), concentrated H₂SO₄ (10 mL), and anhydrous ethanol (*EtOH*, 200 mL) was maintained at reflux under nitrogen for 18 h. After removal of the solvent by rotary evaporation, the resulting mixture was partitioned between H₂O (100 mL) and ether (100 mL). The organic layer was separated and the aqueous layer was further extracted with ether (3 × 100 mL). The combined organic layers were washed with H₂O and brine, dried (Na₂SO₄), and concentrated. Flash chromatography of the residue (SiO₂, 7:3 hexane-ethyl acetate, *EtOAc* dryloaded from acetone) gave the desired ester 2b (6.07 g, 24%) as an orange solid: mp 155–158 °C (literature data [34,35]: 152 °C, 162–163 °C); ¹H NMR (250 MHz, *d*₆-acetone) δ 8.19 and 7.95 (AA'BB' pattern, *J*=8.5 Hz, 4H), 7.92 and 7.06 (AA'BB' pattern, *J*=8.9 Hz, 4H), 4.40 (q, *J*=7.1 Hz, 2H), 1.40 (t, *J*=7.1 Hz, 3H).

2.3. Ethyl 4-(4-dodecyloxyphenylazo)benzoate (2c)

A mixture of 2b (1.00 g, 3.68 mmol), 1-bromododecane (0.90 mL, 3.8 mmol), K₂CO₃ (0.77 g, 5.61 mmol), and *N,N*-Dimethylformamide (*DMF*) (25 mL) was heated to 80 °C under nitrogen for 12 h. After TLC (SiO₂; 70:30 hexane-*EtOAc*) indicated that the reaction was complete, the solvent

was removed in vacuo. The resulting solid residue was partitioned between H₂O (25 mL) and CH₂Cl₂ (25 mL). The organic layer was separated, and the aqueous layer extracted with CH₂Cl₂ (3 × 25 mL). The combined organic layers were washed with water and brine, dried (Na₂SO₄), filtered, and concentrated. Flash chromatography of the residue (SiO₂, 4:1 hexane-ethyl acetate dryloaded in acetone) gave 2c (1.55 g, 96%) as an orange solid: mp 84–86 °C; ¹H NMR (250 MHz, CDCl₃) δ 8.20 and 7.94 (AA'BB' pattern, *J*=9.3 Hz, 4H), 7.94 and 7.01 (AA'BB' pattern, *J*=8.9 Hz, 4H), 4.41 (q, *J*=7.1 Hz, 2H), 4.05 (t, *J*=6.5 Hz, 2H), 1.27–1.86 (overlapped, 23H), 0.88 (t, *J*=5.9 Hz, 3H).

2.4. 4-(4-Dodecyloxyphenylazo)benzoic acid (AA-1)

A slurry of 2c (1.00 g, 2.28 mmol), LiOH (0.27 g, 11.4 mmol), H₂O, and THF (15 mL) was maintained at reflux under nitrogen for 18 h. After TLC (SiO₂; 70:30 hexane-ethyl acetate) indicated that the reaction was complete, the solvent was removed in vacuo. The resulting solid residue was dissolved in H₂O (100 mL) and acidified (conc. H₂SO₄). AA-1 (0.85 g, 90%) was collected as an orange solid through vacuum filtration after recrystallization in acetone: ¹H NMR (500 MHz, CDCl₃, 313K) δ 8.21 (AA'BB' pattern, *J*=8.0, 2H), 7.93 (m, 4H), 7.01 (AA'BB' pattern, *J*=8.5, 2H), 4.06 (t, *J*=6.5, 2H), 1.27–1.50 (overlapped, 20H), 0.88 (t, *J*=6.5, 3H).

2.5. 4-(4-Dodecyloxyphenylazo)phenol (3b)

A mixture of 4-hydroxyazophenol (3a) (1.00 g, 4.66 mmol), K₂CO₃ (1.06 g, 7.62 mmol), 18-crown-6 (cat.), 1-bromododecane (0.39 g, 1.56 mmol), and 100 mL of acetone was maintained at reflux under nitrogen. After TLC (SiO₂; 3:1 hexanes-ethyl acetate) indicated that the reaction was complete, the solvent was removed in vacuo. The resulting mixture was partitioned between H₂O (25 mL) and CH₂Cl₂ (25 mL). The organic layer was separated and the aqueous layer was further extracted with CH₂Cl₂ (3 × 25 mL). The combined organic layers were washed with H₂O and brine, dried (Na₂SO₄), and concentrated. Flash chromatography of the residue (SiO₂, gradient – 100% CH₂Cl₂–>3:1 hexanes:*EtOAc* dryloaded from CH₂Cl₂) gave the desired product 3b (0.39 g, 67%) as a yellow solid: ¹H NMR (250 MHz, CDCl₃) δ 7.86–7.82 (m, 4H), 7.02–6.95 (m, 4H), 4.05 (t, *J*=6.5 Hz, 2H), 1.27–1.86 (overlapped, 20H), 0.88 (t, *J*=5.9 Hz, 3H).

2.6. 4-Oxiranylmethoxyphenyl-4-dodecyloxyphenyldiazene (AE-1)

A mixture of 3b (0.18 g, 0.47 mmol) and K₂CO₃ (0.10 g, 0.71 mmol) in 15 mL of DMF was heated to 85 °C under nitrogen for 1 h. Epichlorohydrin (0.07 g, 0.71 mmol) was added to the mixture and heating was continued. After TLC (SiO₂; 7:3 hexanes-ethyl acetate) indicated that the reaction

was complete, the solvent was removed in vacuo. The resulting mixture was partitioned between H₂O (25 mL) and CH₂Cl₂ (25 mL). The organic layer was separated and the aqueous layer was further extracted with CH₂Cl₂ (3 × 25 mL). The combined organic layers were washed with H₂O and brine, dried (Na₂SO₄), filtered, and concentrated. Flash chromatography of the residue (SiO₂, 7:3 hexanes:EtOAc dryloaded in CH₂Cl₂) gave the desired product (0.28 g, 85%) as a yellow solid: ¹H NMR (250 MHz, CDCl₃) δ 7.86–7.82 (m, 4H), 7.02–6.95 (m, 4H), 4.32–4.26 (dd, *J* = 3.1 Hz, 1H), 4.03–3.97 (m, 3H), 3.40–3.34 (m, 1H) 2.93–2.90 (m, 1H), 2.79–2.76 (m, 1H), 1.27–1.86 (overlapped, 20H), 0.88 (t, *J* = 5.9 Hz, 3H).

Monomolecular films of the amphiphilic compounds were prepared by the Langmuir technique on an RK-1 trough (Riegler and Kirstein, GmbH) located in a laminar flow hood. The compounds were dissolved in chloroform (Fisher, reagent grade) to concentrations of 0.5–1.0 mmol/L. The solution was spread over the water subphase (NanoPure, >18 MΩ × cm). Monolayers were deposited on a cleaned silicon wafer [36,37] (Semiconductor Processing Co.) of the {100} orientation, following the usual LB procedure [38].

Liquid surface measurements were performed on monomolecular films spread on a temperature controlled, custom-built Teflon trough. To reduce the background scattering and oxidation of the monolayer, the trough was placed in a helium-filled chamber for the duration of the experiments. A combination of grazing incident X-ray diffraction (GIXD) (in-plane and rod-scans) and X-ray reflectivity experiments were conducted on a liquid–surface X-ray spectrometer at the 6ID beam line at the Advanced Photon Source synchrotron at Argonne National Laboratory according to the usual procedure [39–41]. A downstream Si double crystal monochromator was used to select the X-ray beam at the desired energy ($\lambda = 0.0772$ nm).

Experimental setup and details regarding the X-ray reflectivity and GIXD were described in previous publications [24,25]. The box model was used to determine the electron densities across the interface and to relate them to the molecular arrangements of the molecular fragments at the interface [42]. The box model consisted of slabs of differing thickness and electronic density stacked above the water subphase with known electron density (0.33 e/Å³). The interfaces were smeared to account for the surface roughness and thermal vibrations. The arrangement of the molecular segments was determined from the length and electron density of the boxes via direct comparison with molecular models. The reflectivity used to fit the experimental data was calculated from:

$$R(Q_z) = R_0(Q_z)e^{-(Q_z\sigma)^2} \quad (1)$$

where the $R_0(Q_z)$ is the reflectivity from step-like functions and σ is the surface roughness. The reflectivity calculated for various trial electronic density profiles was compared with experimental results during the fitting procedure.

The UV–vis spectra of 0.01 mmol/L solutions in chloroform were obtained with a Shimadzu-1601 spectrometer. A Blak-Ray ultraviolet lamp (UVP, Model B-100 AP, 100 W) equipped with both a 365 nm bandpass filter and a 310 nm longpass filter was used to illuminate the solutions at a distance of 0.4 m. Ellipsometric measurements of monolayer thickness were performed on a COMPEL Automatic Ellipsometer (InOmTech, Inc.). Imaging of the monolayers was carried out by atomic force microscopy (AFM) (Multimode and Dimension-3000, Digital Instruments), using non-contact silicon V-shaped cantilevers (Veeco Instruments, typical spring constant 48 N/m) with an average tip radius of 25–30 nm determined by scanning a gold nanoparticle reference sample [43]. All AFM images were obtained using light tapping mode, directed by the setpoint ratio (rsp), defined as the ratio of the operating setpoint to the free oscillating amplitude of the cantilever [44,45]. In light-tapping, the tip sample interaction is strongly influenced by adhesion and the phase shift is greater on the surface with areas of higher attractive forces, whereas in the hard-tapping regime the elastic response becomes predominant [46]. The morphology of the surface layers was probed at several random locations with widely varying scan sizes from 0.1 to 30 μm. The geometrical parameters of all molecules were estimated from molecular models built with the Cerius² 3.8 package on a SGI workstation by using the Dreiding 2.21 force field library and with the Materials Studio 3.0 package on a PC workstation using the PVCC force field library. Molecular models were treated with a molecular dynamics and a minimization procedure to obtain conformations with minimized energy.

3. Results and discussion

4-(4-dodecyloxyphenylazo)benzoic acid (AA-1) and 4-(4-dodecyloxyphenylazo)benzoic epoxy (AE-1) both possess a dodecyl tail attached to an azobenzene group but vary in the nature of the head group: a standard carboxyl group (AA-1) and a much bulkier epoxy group (AE-1) directly attached to the azobenzene fragment (Fig. 1). The photoisomerization of both molecules in dilute solution was confirmed using UV–vis spectroscopy (Fig. 2). Under ambient conditions the characteristic $\pi - \pi^*$ absorbance at 365 nm was observed, indicative of the *trans*-isomer of the azobenzene fragment (Fig. 2) [47,48]. After one minute illumination, the absorbance at 365 nm was replaced with two strong bands at 318 and 455 nm, indicating a predominant transformation to the *cis*-isomer. Therefore, the presence of bulky epoxy terminal groups does not suppress the photoisomerization ability of the azobenzene groups in these novel compounds. Further photoisomerization studies and discussion will be presented in future communications [49].

The behavior of the azobenzene amphiphiles with different polar heads was first deduced by comparison of the pressure versus area ($\pi - A$) isotherms. The $\pi - A$ isotherms for AA-1 and AE-1 indicated cross-sectional

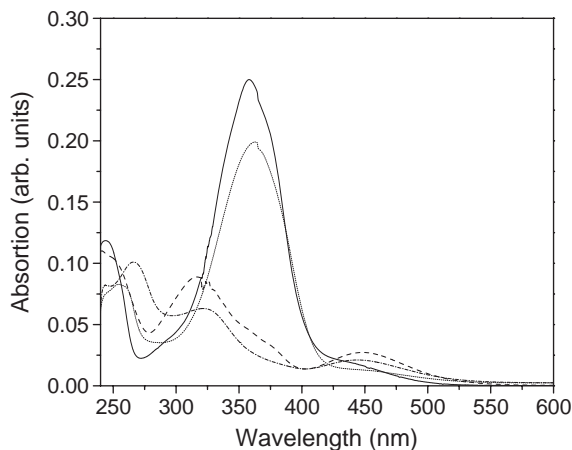


Fig. 2. UV-vis spectra for AA-1 (dotted line) and AE-1 (solid line) under ambient light and for AA-1 (dash-dot line) and AE-1 (dashed line) after one minute illumination by 365 nm light.

areas corresponding to the polar head size (Fig. 3). The limiting cross-sectional area was calculated from the isotherms as 0.24 nm^2 for AA-1 and 0.28 nm^2 for AE-1, which was slightly larger than the molecular area for traditional aliphatic chain amphiphiles [50,51]. Traditional amphiphiles composed of an alkyl tail and carboxylic acid polar head have been estimated to occupy approximately $0.18\text{--}0.20 \text{ nm}^2$ per molecule in condensed state [52]. The inclusion of the azobenzene fragment has been observed to increase the cross-sectional area of the single alkyl tail amphiphile to $0.30\text{--}0.35 \text{ nm}^2$ per molecule [53]. The smaller than expected molecular areas obtained for both molecules studied here suggested that this combination of the azobenzene group and polar heads dictate different intramonomer packing as will be discussed in this communication. The collapse of the AA-1 monolayer at moderate surface pressures was observed as a sharp change of slope at 25 mN/m . The larger surface area per molecule in AE-1 (by $\sim 15\%$) can be directly associated with the presence of the bulkier epoxy groups at the interface. The

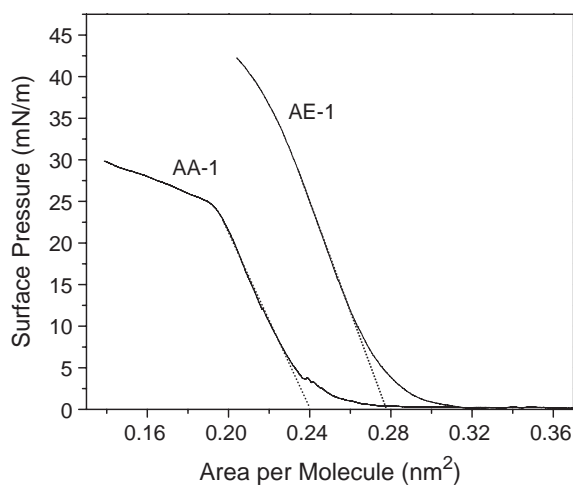


Fig. 3. π -A isotherms for molecules AA-1 and AE-1. The tangent lines indicate the corresponding A_0 .

epoxy head group was suggested to be stable at the air-water interface for the limited time scale of the experiments. Epoxy rings were determined to be relatively stable in gels with high water content with only 10% of the rings opening after 24 h in the absence of a catalyst and at room temperature [54]. Therefore, we presume a minimum number of epoxy rings open during the 1–10 h per each experiment in oxygen-free environment. In fact, the result reported here for AE-1 show unchanged monolayer packing in the course of repeated measurements.

Diffraction experiments provided insight into the effect of the azobenzene group and polar head on the intralayer structure of the alkyl tails. Observational GIXD patterns for both molecules at all surface pressures indicated an orthorhombic unit cell for the AA-1 and AE-1 molecules (Figs. 4a, 5a). Four intense peaks appeared at low surface pressures and sharpened as the surface pressure increased.

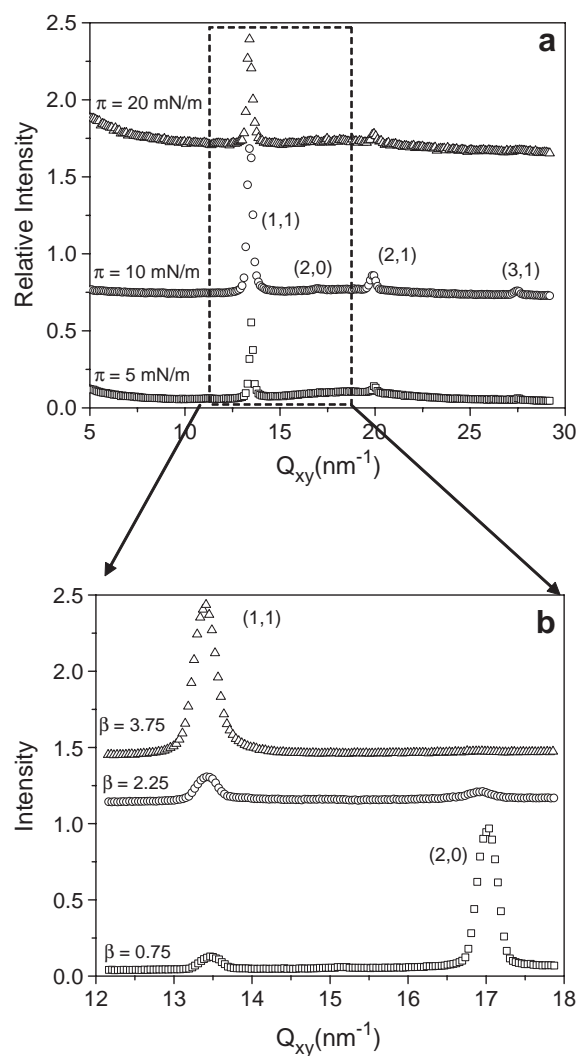


Fig. 4. Intensity versus in-plane momentum transfer Q_{xy} GIXD (at $\beta = 3.75^\circ$ to show all visible peaks) for AA-1 a) at all observed surface pressures and b) the highest pressure at increased resolution. The dashed box indicates the area shown at higher resolution for different β to reveal the selective appearance of the (1,1) and (2,0) peaks. The intensities were offset to allow comparison.

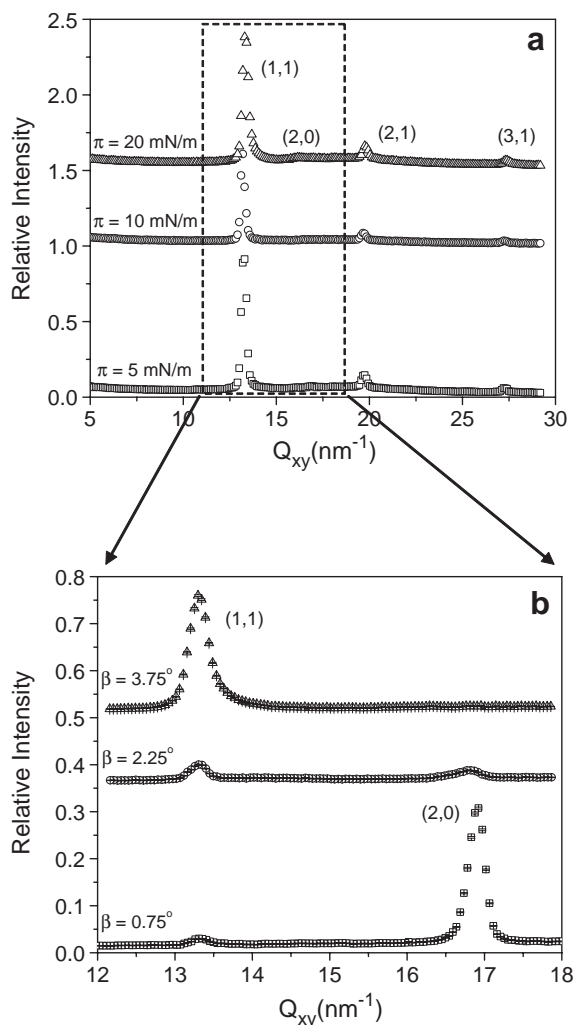


Fig. 5. Intensity versus in-plane momentum transfer Q_{xy} . GIXD (at $\beta = 3.75^\circ$ to show all visible peaks) for AE-1 a) at all observed surface pressures and b) the highest pressure at higher resolution. The dashed box indicates the area shown at higher resolution for different β to reveal the selective appearance of the (1,1) and (2,0) peaks. The intensities were offset to allow comparison.

The diffraction curve fitting was conducted using Lorentzian functions in all cases. At lower β a single sharp, intense peak was observed while at higher β three additional intense peaks were observed for both AA-1 and AE-1 molecules. Unlike the previously studied molecule with a bulky crown ether polar head AD12-1 [24], the current molecules lacked lower Q_{xy} peaks, indicating an absence of supercell packing structure.

The d-spacings for the two lower Q_{xy} peaks observed for AA-1 were calculated as 0.467 and 0.371 nm corresponding to an orthorhombic unit cell with $a = 0.742$ nm and $b = 0.601$ nm at all surface pressures. The area per alkyl chain calculated from this unit cell was 0.223 nm^2 which is close to that directly obtained from Langmuir isotherms (Table 1). The large spacing between the two characteristic peaks for the orthorhombic unit cell indicated a transition to a unit cell of lower symmetry than the hexagonal unit cell

(Fig. 4b). Indeed, the area per alkyl chain was much larger than previously seen for single alkyl chains [55]. The additional peaks observed in the GIXD pattern were found to have a higher order of diffraction relationship with the orthorhombic unit cell.

The d-spacings of the higher Q_{xy} peaks were calculated to be 0.316 and 0.229 nm and indexed as the second order (2,1) and (3,1) peaks, respectively (Fig. 4a). The appearance of these additional peaks for higher azimuthal angles indicated the diffraction from higher orders of symmetry than traditionally seen for simple amphiphiles such as a herringbone structure. The appearance of the (2,1) peak is typically forbidden for a non-primitive orthorhombic lattice along with the (0, 1) peak unless the two interpenetrating rectangular lattices were laterally shifted from one another or the two molecules per unit cell were not symmetrically equivalent [21]. However, the absence of the (0,1) peak suggested the alkyl tails of AA-1 molecules formed a herringbone structure at the air–water interface. The (1,1), (2,1) and (3,1) peaks were weak but observable at lower Q_z and sharply increased in intensity at higher Q_z while the (2,0) peak was absent at higher Q_z GIXD patterns. This selective appearance of the peaks elucidated the alkyl tails were tilted towards the nearest neighbor (NN) direction [18,21].

The increase in the cross-sectional area of the polar head from a carboxyl group to an epoxy group led increased surface molecular areas as was mentioned above (Fig. 3). Correspondingly, a slight shift in the diffraction peaks toward lower Q_{xy} was observed for AE-1 at all surface pressures (Fig. 5a). The four peaks were observed at 0.472, 0.372, 0.319, and 0.231 nm and indexed as the (1,1), (2,0), (2,1) and (3,1) peaks, respectively at 20 mN/m (Table 1). The characteristic peaks were spaced further apart than the AA-1 peaks, thus, resulting in unit cell parameters of $a = 0.744$ nm and $b = 0.611$ nm. The area per alkyl tail was determined to be 0.227 nm^2 , a value larger than expected for traditional orthorhombic unit cells. Similar to the AA-1 molecule, the presence of high orders of reflections signified

Table 1

Structural parameters of Langmuir monolayers from different photochromic amphiphiles at highest surface pressure (20 mN/m pressure)

	Stearic acid [55]	AA-1	AE-1	AD12-1 [24]
<i>d-spacings, (nm)</i>				
(1,1) peak	0.424	0.467	0.472	0.440
(2,0) peak	0.418	0.371	0.372	0.394
<i>Unit cell parameters</i>				
a (nm)	0.836	0.742	0.744	0.788
b (nm)	0.483	0.601	0.611	0.529
Area per chain (nm^2)	0.197	0.223	0.227	0.208
Chain tilt ($^\circ$)	16.5	35	42	58
<i>Correlation length (nm)</i>				
(1,1) peak		9.3	7.2	16.5
(2,0) peak		11.3	10.4	17.1

Intramonomer parameters.

a high ordering of the alkyl tails. Therefore, the tails were concluded to be aligned in a moderately tilted packing structure due to the selective appearance of the peaks. As in the GIXD patterns for the AA-1 molecules, the (1,1), (2,1), and (3,1) peaks appeared as weak peaks at lower β and became sharper and more intense at higher β . Dissimilarly however, the (2,0) peak appeared sharp and intense at lower β and disappeared at higher β . From the selective appearance of the indexed peaks it was determined the alkyl chains were tilted in the NN direction similarly to the AA-1 molecules.

The higher resolution GIXD pattern at 20 mN/m for AA-1 and AE-1 shown in Figs. 4b, 5b indicated the highly selective appearance of the (1,1) and (2,0) peaks as the detector was moved further away from the horizon. The data for both molecules at higher β showed the (2,0) peak became much less intense while the (1,1) peak increased in intensity, indicating the alkyl tails were tilted in the (1,1) direction. The increase in spacing between the two characteristic peaks observed for the AE-1 molecule corroborated the increase in the cross-sectional area per alkyl tail. The AA-1 and AE-1 molecules were found to have moderate long-range order. The correlation lengths calculated for the (1,1) peaks were 9.3 and 7.2 nm for AA-1 and AE-1, respectively (Table 1). The molecules had

increased correlation lengths in the (2,0) direction, seen in the sharpening of the peaks in Figs. 4b, 5b.

The orthorhombic unit cells suggested for the AA-1 and AE-1 molecules from GIXD data are considerable larger than the unit cell calculated for stearic acid molecules with comparable alkyl tails (Table 1). Both molecules show a decrease in the a dimension and an increase in the b dimension of the unit cells. The area per alkyl chain increases from 0.197 nm², for the stearic acid molecule, to 0.223 and 0.227 nm² for the molecules with carboxyl and epoxy head groups, respectively (Table 1). The larger unit cells suggest the azobenzene group interfered with the intralayer packing of the alkyl tails since the polar head itself cannot generate a larger cross-sectional area. The most noticeable is that the alkyl tails for AA-1 and AE-1 are packed in a herringbone manner (Fig. 6). We suggest that the presence of the azobenzene group created two symmetrically inequivalent sites and enlarged the orthorhombic unit cell along the b -axes by initiating their larger tilt towards the NN direction (Fig. 6). The cross-sectional areas determined by the $\pi \sim A$ isotherm for AA-1 and AE-1 were calculated to be 0.25 and 0.29 nm² in the beginning of the formation of the condensed monolayer and decreasing to 0.20 and 0.23 nm² closer to the monolayer collapse, respectively. The known cross-sectional area for azobenzene

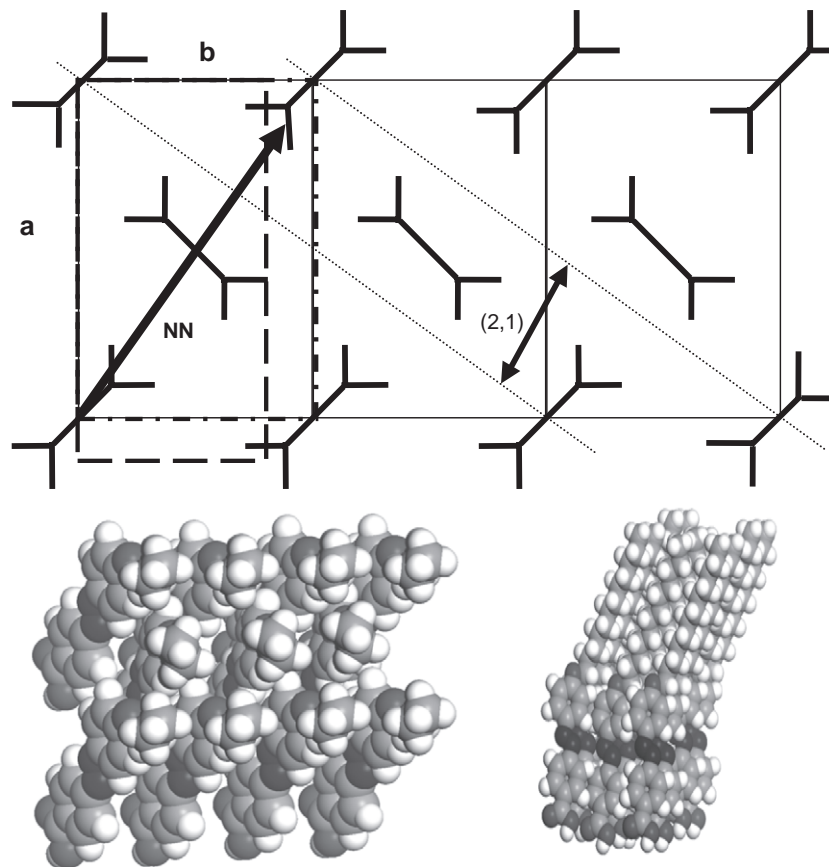


Fig. 6. Unit cell comparison of AA-1 (solid line, clear herringbone packing), AE-1 (dashed line), and stearic acid (dashed dotted line) from literature [55] (top, left cell). The AA-1 is expanded in the b direction to demonstrate the (2,1) plane (diagonal lines). Molecular model of AA-1 organized in three unit cells viewed along the alkyl tails (bottom left) and side-view (bottom right).

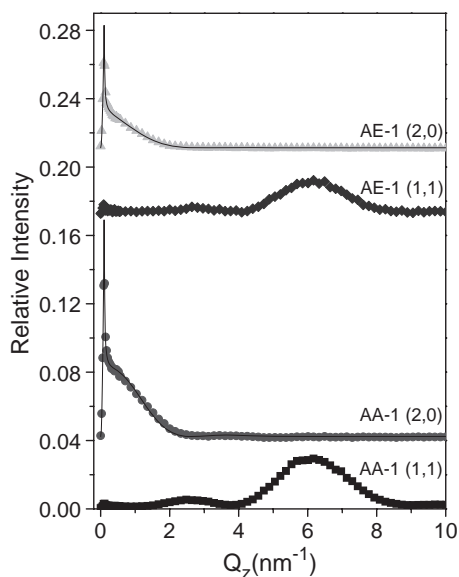


Fig. 7. Rod scans of (1,1) and (2,0) peaks for AA-1 and AE-1 at 20 mN/m. The data represented by symbols and model fits are shown by lines.

groups was between 0.30 and 0.35 nm², which was slightly larger than the cross-sectional area for the carboxyl group (0.24 nm²) but fairly comparable for the epoxy polar group (0.30 nm²) [52]. The effect was not seen for the larger AD12-1 molecule (Table 1), indicating the larger polar head decreased the interference from the azobenzene group.

Independent confirmation of the larger tilt angle and information about the tilt direction of the alkyl tails was determined from rod scans of the two most intense diffraction peaks observed for each molecule. The rod scans for AA-1 and AE-1 molecules in the (2,0) direction displayed the angular behavior with a sharp peak prior to a gradual decrease in intensity, while for the rod scans of the lower Q_{xy} peak, the tilt projection shown along the (1,1) direction confirmed the nearest neighbor tilt direction (Fig. 7). Modeling of the rod-scan data for AA-1 and AE-1 confirmed the tails tilted approximately 35° and 42°, respectively (Table 1). The tilt behavior of AA-1 and AE-1 in NN direction differed from the corresponding behavior for photochromic amphiphiles with shorter alkyl tails and flexible spacer between azobenzene group and polar head. Durbin et al. observed a transition in the tilt direction of the molecules from the NN direction to the next nearest neighbor (NNN) while the tilt angle remained constant [56]. The azobenzene fragment was found to influence the cross-sectional area of the molecules while the van der Waals attraction between the short alkyl chains determined the packing structure of the molecules. Comparison with the bulk structure of azobenzene groups found the amphiphilic molecules formed a lattice structure of the H-aggregates of the photochromic group. In contrast, the amphiphilic molecules observed in this study appeared to show no transition from the NN to the NNN direction; however, the tilt angle correlated with the angles observed for both the

shorter chain amphiphiles at the air–water interface and literature values for the bulk structure of azobenzene groups [56,57].

Further observations of the Langmuir monolayers of AA-1 and AE-1 molecules were performed by X-ray reflectivity. The data for both molecules showed a single well-defined minimum and an additional subtle minima observed at the highest surface pressures (Fig. 8). A two box model was used to fit the data for both molecules at all observed surface pressures where the first box was assigned to the hydrophilic polar head and azobenzene group and the second box was assigned to the hydrophobic alkyl tails (Fig. 9). Ideally the molecule would be modeled using a three box model but the short length of the focal group and the lower resolution of the experimental setup led to the inclusion of the hydrophilic polar head and the azobenzene fragment in the first box.

The decrease in spacing for the defined minima for increasing surface pressure indicated an increase in the thickness of the head group box from 1.17 to 1.46 nm for AA-1 (Table 2, Fig. 8a). The change in thickness suggested the azobenzene group transitioned from 33.3° tilt from the

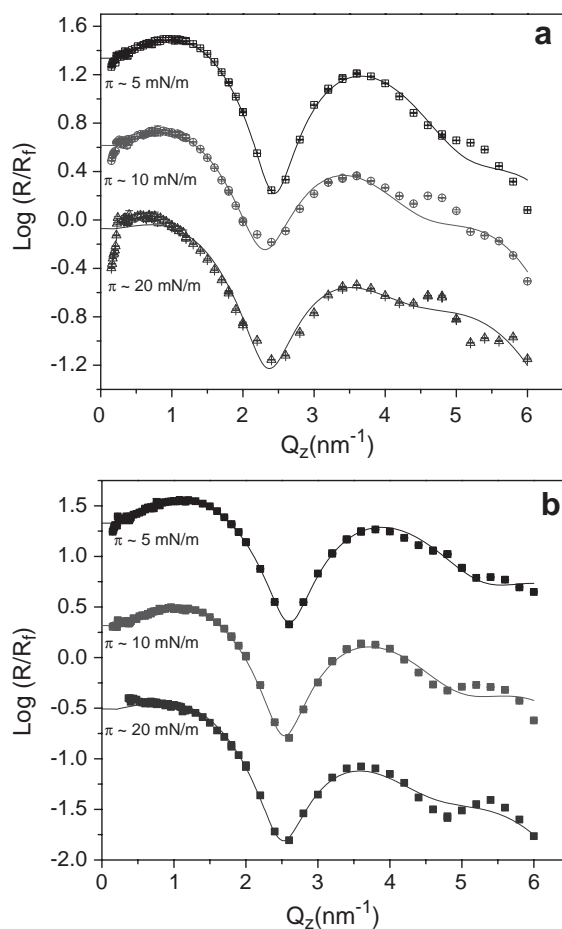


Fig. 8. Normalized reflectivity data for a) AA-1 and b) AE-1 at different surface pressures observed. The experimental data were offset for clarity and were represented by symbols and fits are represented by lines.

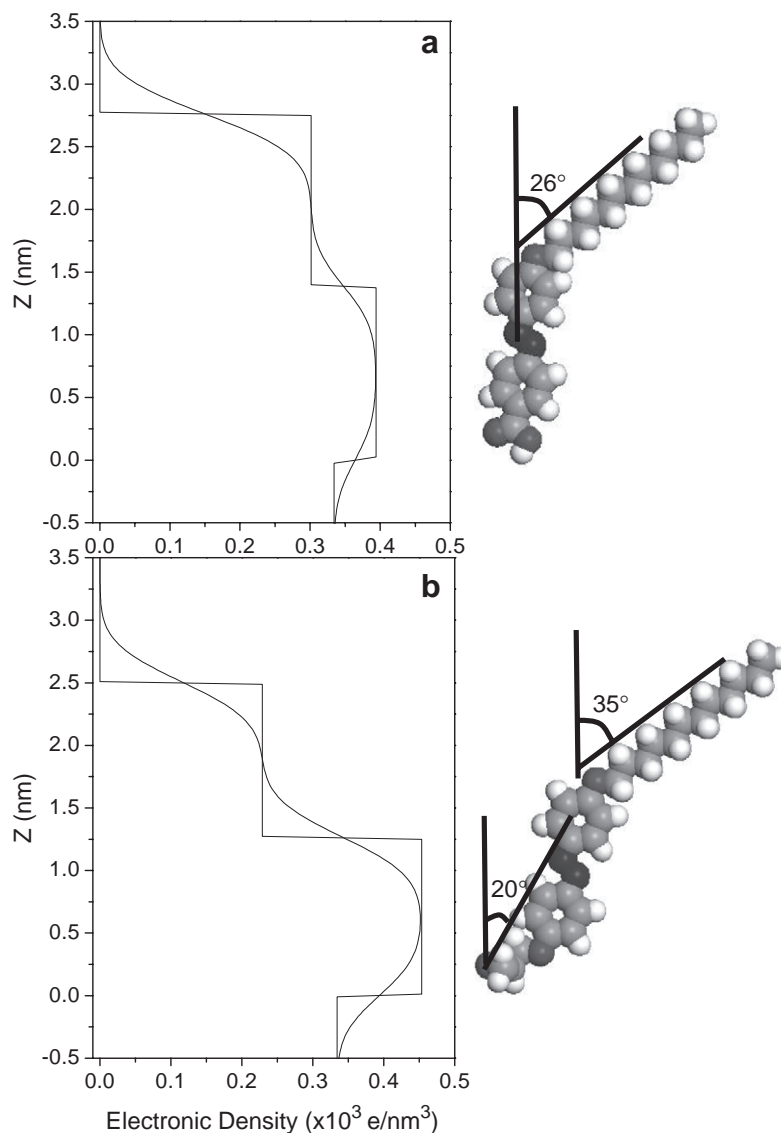


Fig. 9. Box model for molecules a) AA-1 and b) AE-1 in condensed state at 10 mN/m (left) and corresponding molecular models (right).

surface normal to virtually vertical orientation (Table 2). The electron density for the first box was higher than calculated for densely packed azobenzene fragment and carboxylic acid polar heads, confirming the presence of

water molecules. The attraction between the hydrophilic head group and the water subphase forced the head group to submerge into the subphase and pack partially below the air–water interface. Unlike the azobenzene group, the

Table 2

Parameters of box models calculated from the X-ray reflectivity data for molecules AA-1 and AE-1 at different surface pressures

Sample	AA-1			AE-1		
Surface pressure (mN/m)	5	10	20	5	10	20
Head box length (± 0.03 nm)	1.17	1.39	1.46	1.18	1.27	1.39
Head box electronic density ($\pm 0.02 \times 10^3$ e/nm ³)	0.42	0.39	0.40	0.47	0.45	0.41
Tail box length (± 0.03 nm)	1.36	1.37	1.32	1.22	1.24	1.24
Tail box electronic density ($\pm 0.02 \times 10^3$ e/nm ³)	0.31	0.30	0.18	0.24	0.23	0.19
Surface roughness (± 0.04 nm)	0.261	0.258	0.269	0.218	0.249	0.302
Total thickness (± 0.06 nm)	2.53	2.76	2.78	2.40	2.51	2.63
Azobenzene tilt angle ($\pm 3.0^\circ$)	33	18	0	37	31	20
Tail tilt angle ($\pm 3.0^\circ$)	26	26	26	35	35	35

Layered ordering.

thickness of the second box remained virtually unchanged around 1.35 nm, suggesting the alkyl tails remained tilted at 25.7° from the surface normal at all surface pressures (Table 2). The difference in the tilt angle, determined from rod scans and reflectivity data, was within the uncertainties of both measurements.

The area per alkyl tail projected along the AA-1 molecular axes was calculated by $A=A_0\cos(\theta)=0.25\cos(25.7)=0.225\text{ nm}^2$, comparable to the area per tail calculated by GIXD (0.223 nm^2) (Table 1). The electronic density for the alkyl tails' box was lower than that calculated for densely packed alkyl chains. However, the density calculated by the box model was equivalent to the density calculated from molecular models of the tilted molecules. Both boxes were observed to decrease in electronic density at 20 mN/m. The monolayer was previously discerned to undergo a collapse at 25 mN/m as was concluded from the $\pi-A$ isotherm (Fig. 3). The large decrease in the electronic density of the box model indicated the alkyl tails form cluster packing prior to the complete collapse of the monolayer.

Similar to the AA-1 molecule, for the AE-1 molecule at rising compression the X-ray reflectivity data showed a well-defined minimum, indicating an increase in the head group box thickness from 1.18 to 1.39 nm (Table 2, Fig. 8b). Unlike the AA-1 molecule, the orientation of the azobenzene group for AE-1 was calculated to be changed from 37.2° at low surface pressure to 20.1° at 20 mN/m. This difference demonstrates the role of the larger epoxy polar head group which induced a larger tilt angle of the azobenzene group that could not easily be changed by the monolayer compression. Moreover, the head group box possessed higher electronic density confirming the presence of water molecules packed among the epoxy head groups and overall denser packing of these fragments (Table 2). Additionally, the box model showed the thickness of the second box was approximately 1.24 nm for all pressures, thereby indicating the alkyl tails to be tilted 35.3° from the surface normal at all pressures, while forming a kinked structure. The overall thickness of the monolayer is substantially (0.1–0.2 nm) smaller for AE-1 molecules (Table 2). The projected cross-sectional area per alkyl tail (0.228 nm^2) was comparable to the area per tail (0.227 nm^2) determined by GIXD. The larger azobenzene group and the epoxy polar head forced a larger cross-sectional area, as was concluded from the $\pi-A$ isotherm (Fig. 3). The larger cross-sectional area then forced the alkyl tails to tilt further to achieve the preferred densely packed structure. However the alkyl tail box had a lower electronic density than predicted for densely packed, tilted alkyl tails. This lower than expected electronic density suggested the tails formed a cluster structure at the air–water interface.

Comparison of the box models for the moderate surface pressure demonstrated the influence of polar head groups on the overall molecular conformation as presented in Fig. 9 for individual molecules (see Fig. 6 for densely packed monolayers). The thickness of the alkyl tail boxes for both

molecules proved the tails remained tilted although the cross-sectional area decreased. Conversely, the carboxylic head group and azobenzene fragment of the AA-1 shifted from a tilt angle similar to the alkyl tails to a virtually vertical orientation (Fig. 9a). Dissimilarly, the epoxy head group and azobenzene fragment of the AE-1 molecule still remained significantly tilted in the condensed state (Fig. 9b). The tilt of the alkyl tail becomes much larger in AE-1 monolayer. This represents significant difference in the intramonolayer packing of the two molecules which can improve the ability of the azobenzene group attached to the bulkier epoxy heads for photoisomerization in a condensed state.

The deposition of the monolayer on solid supports provided further insight in the two-dimensional morphology of the monolayer (Fig. 10). AFM imaging of the deposited AA-1 monolayers showed the domain formation prior to the monolayer collapse with lateral domain dimensions below $1\text{ }\mu\text{m}$. The monolayers deposited at 5 mN/m appeared uniform with an effective thickness of 2.3 nm and a surface roughness of 0.35 nm which are fairly close to that determined from X-ray data at the air–water interface (Table 2). A moderate increase in surface pressure did not disrupt the uniform film and also showed negligible changes in monolayer thickness and surface roughness. At higher surface pressures, a second domain layer appeared to form on top of the monolayer (Fig. 10a).

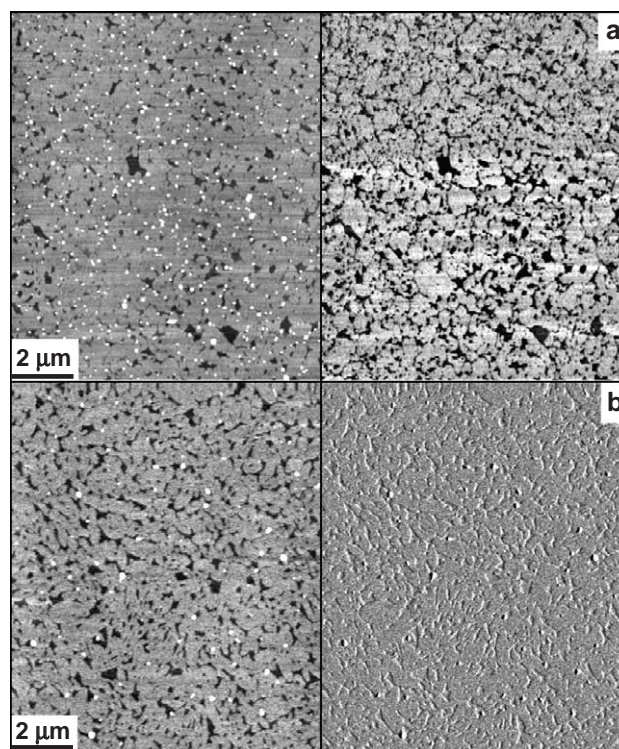


Fig. 10. AFM images for LB monolayer formed from large domains for a) AA-1 at 20 mN/m and b) AE-1 at 30 mN/m. The z-range for topography (left images) was 5 nm and the z-range for phase (right images) was a) 30° and b) 5° .

Unlike the AA-1 molecule, AE-1 molecules formed a monolayer with a domain structure at all observed pressures. The surface coverage increased at the highest pressures as the overall size of the domains decreased, although the shape and structure of the semi-continuous domains with lateral dimensions below 1 μm remained unchanged (Fig. 10b).

4. Conclusions

In conclusion, we observed significant differences in the two-dimensional packing structure of photochromic amphiphiles with different polar heads. At the air–water interface, the AA-1 and AE-1 molecules formed orthorhombic packing structures with larger than expected areas per molecule and higher orders of symmetry than traditional amphiphiles composed of a single alkyl tail and a compact polar head. The azobenzene group forced the alkyl tails to form a herringbone structure with modest long range order. Unlike molecules with a short (C_6) chain attached to an azobenzene fragment, the AA-1 and AE-1 molecules were observed to tilt in the NN direction at all pressures. The molecule with the carboxylic acid head group had a smaller tilt angle than that observed for either the epoxy terminated molecule or the bulk azobenzene structures. The tail of the AA-1 molecule was determined to be tilted 25° from the surface normal while the tail of the AE-1 molecule was tilted at much larger angle, approximately 35° . In addition to the tilted alkyl tails, the azobenzene group of the AE-1 molecule in condensed monolayer was significantly tilted in contrast with AA-1 molecules with virtually vertical orientation of the azobenzene group. This represents a significant difference in the intramonolayer packing of two molecules which can enhance the ability of the azobenzene group terminated with the epoxy head for photoisomerization in the condensed state. Considering that the molecule AE-1 is more loosely packed and tilted, we can suggest that the photoisomerization reaction which requires more free volume will be more efficient in this compound. The study of the grafting ability of this compound and its photoisomerization behavior in solid monolayer state is in progress.

Acknowledgements

The authors thank M. Ornatska, S. Peleshanko, and B. Rybak for technical assistance. Funding from the National Science Foundation (DMR-038982) is gratefully acknowledged. The Midwest Universities Collaborative Access Team (MUCAT) sector at the APS is supported by the U.S. Department of Energy, Basic Energy Sciences through the Ames Laboratory under Contract No. W-7405-Eng-82. Use of the Advanced Photon Source was supported by the U.S. Department of Energy, Basic Energy Services, Office

of Science, under Contract No. W-31-109-Eng-38. OFV is a Sloan Foundation Scholar.

References

- [1] T. Ikeda, *J. Mater. Chem.* 13 (2003) 2037.
- [2] H. Nishihara, *Bull. Chem. Soc. Jpn.* 77 (2004) 407.
- [3] V. Shibaev, A. Borbovsky, N. Boiko, *Prog. Polym. Sci.* 28 (2003) 729.
- [4] T. Seki, in: H.S. Nalwa (Ed.), *Handbook of Photochemistry and Photobiology*, American Scientific Publishers, California, 2003, p. 435.
- [5] S.K. Yesodha, S.K. Sadashiva Pillai, N. Tsutsumi, *Prog. Polym. Sci.* 29 (2004) 45.
- [6] V.V. Tsukruk, V.N. Bliznyuk, *Prog. Polym. Sci.* 22 (1997) 1089.
- [7] P. Rochon, E. Batalla, A. Natanson, *Appl. Phys. Lett.* 66 (1995) 136.
- [8] D.Y. Kim, S.K. Li, L. Tripathy, J. Kumar, *Appl. Phys. Lett.* 66 (1995) 1166.
- [9] S. Kawata, Y. Kawata, *J. Opt. Soc. Am. B* 18 (2001) 1777.
- [10] X. Meng, A. Natansohn, C. Barrett, P. Rochon, *Macromolecules* 29 (1996) 946.
- [11] M. Ho, A. Natansohn, C. Barrett, P. Rochon, *Can. J. Chem.* 73 (1995) 1773.
- [12] A. Natansohn, P. Rochon, M. Ho, C. Barrett, *Macromolecules* 28 (1995) 4179.
- [13] K. Ichimura, *Chem. Rev.* 100 (2000) 1847.
- [14] T. Yamaoka, Y. Makita, H. Sasatani, S.-I. Kim, Y. Kimura, *J. Control. Release* 66 (2000) 187.
- [15] T. Seki, J. Kojima, K. Ichimura, *Macromolecules* 33 (2000) 2709.
- [16] T. Seki, H. Sekizawa, R. Fukuda, T. Tamaki, M. Yokoi, K. Ichimura, *Polym. J.* 28 (1996) 613.
- [17] T. Seki, H. Sekizawa, R. Fukuda, S. Morino, K. Ichimura, *J. Phys. Chem.* 102 (1998) 5313.
- [18] M. Kaganer, E.B. Loginov, *Phys. Rev., E* 51 (1995) 2237.
- [19] V.M. Kaganer, M.A. Osipov, *J. Chem. Phys.* 109 (1998) 2600.
- [20] V.M. Kaganer, G. Brezesinski, H. Mohwald, P.B. Howes, K. Kjaer, *Phys. Rev., E* 59 (1999) 2141.
- [21] P. Dutta, *Colloids Surf., A* 171 (2000) 59.
- [22] W.-J. Pao, F. Zhang, P.A. Heiney, C. Mitchell, W.D. Cho, V. Percec, *Phys. Rev., E* 67 (2003) 021601.
- [23] W.-J. Pao, M.R. Stetzer, P.A. Heiney, W.-D. Cho, V. Percec, *J. Phys. Chem. B* 105 (2001) 2170.
- [24] K. Larson, D. Vaknin, O. Villavicencio, D.V. McGrath, V.V. Tsukruk, *J. Phys. Chem.* 106 (2002) 7246.
- [25] K.L. Genson, D. Vankin, O. Villavicencio, D.V. McGrath, V.V. Tsukruk, *J. Phys. Chem.* 106 (2002) 11277.
- [26] A. Sidorenko, C. Houphouet-Boigny, O. Villavicencio, M. Hashemzadeh, D.V. McGrath, V.V. Tsukruk, *Langmuir* 16 (2000) 10569.
- [27] V.V. Tsukruk, I. Luzinov, K. Larson, S. Li, D.V. McGrath, *J. Mater. Sci. Lett.* 20 (2001) 873.
- [28] I. Luzinov, D. Julthongpipit, A. Liebmann-Vinson, T. Cregger, M.D. Foster, V.V. Tsukruk, *Langmuir* 16 (2000) 504.
- [29] I. Luzinov, D. Julthongpipit, H. Malz, J. Pionteck, V.V. Tsukruk, *Macromolecules* 33 (2000) 1043.
- [30] E. Atkinson, H.J. Lawler, J.C. Heath, E.H. Kimball, E.R. Read, *J. Am. Chem. Soc.* 63 (1941) 730.
- [31] S. Shinkai, K. Shigematsu, T. Ogawa, T. Minami, O. Manabe, *Tetrahedron Lett.* 21 (1980) 4463.
- [32] W.C. Still, M. Kahn, A. Mitra, *J. Org. Chem.* 43 (1978) 2923.
- [33] L. Corvazier, Y. Zhao, *Macromolecules* 32 (1999) 3195.
- [34] I.M. Roushdi, R. Soliman, *U.A.R. J. Chem.* 13 (1970) 399.
- [35] I.K. Feldman, C.S. Frankowskii, *J. Gen. Chem. USSR* 33 (1963) 893, (Engl. Transl.).
- [36] V.N. Bliznyuk, M.P. Everson, V.V. Tsukruk, *J. Tribol.* 120 (1998) 489.
- [37] V.V. Tsukruk, *Adv. Mater.* 13 (2001) 95.
- [38] A. Ulman, *An Introduction to Ultrathin Organic Films*, Academic Press, San Diego, CA, 1991.

- [39] D. Vaknin, in: E.N. Kaufmann, R. Abbaschian, P.A. Baines, A.B. Bocarsly, C.L. Chien, B.L. Doyle, B. Fultz, L. Leibowitz, T. Mason, J.M. Sanches (Eds.), *Method of Materials Research*, John Wiley Sons, New York, 2001, p. 10d.2.1.
- [40] I. Weissbuch, F. Leveiller, D. Jacquemain, K. Kjaer, J. Als-Nielsen, L. Leiserowitz, *J. Phys. Chem.* 97 (1993) 12858.
- [41] D. Vaknin, M.S. Kelley, *Biophys. J.* 79 (2000) 2616.
- [42] B.W. Gregory, D. Vaknin, J.D. Gray, B.M. Ocko, P. Stroeve, T.M. Cotton, W.S. Struve, *J. Phys. Chem. B* 101 (1997) 2006.
- [43] M. Radmacher, R.W. Tilmann, H.E. Gaub, *Biophys. J.* 64 (1993) 735.
- [44] V.V. Tsukruk, *Rubber Chem. Technol.* 70 (1997) 430.
- [45] V.V. Tsukruk, D.H. Reneker, *Polymer* 36 (1995) 1791.
- [46] S.N. Magonov, J. Cleveland, V. Elings, D. Denley, M.H. Whangbo, *Surf. Sci.* 389 (1997) 201.
- [47] S. Peleshanko, A. Sidorenko, K. Larson, O. Villavicencio, M. Ornatka, D.V. McGrath, V.V. Tsukruk, *Thin Solid Films* 406 (2002) 233.
- [48] A. Sidorenko, C. Houphouet-Boigny, O. Villavicencio, D.V. McGrath, V.V. Tsukruk, *Thin Solid Films* 410 (2002) 147.
- [49] K.L. Genson, J. Holzmüller, O. Villavicencio, D.V. McGrath, D. Vaknin, V.V. Tsukruk, *J. Phys. Chem.* (2005).
- [50] I.R. Peterson, *J. Phys. D. Appl. Phys.* 23 (1990) 379.
- [51] V.M. Kaganer, H. Möhwald, P. Dutta, *Rev. Mod. Phys.* 71 (1999) 779.
- [52] G. Weidemann, G. Brezesinski, D. Vollhardt, H. Mohwald, *Langmuir* 14 (1998) 6458.
- [53] T. Seki, F. Takashi, I. Kunihiro, *Bull. Chem. Soc. Jpn.* 71 (1998) 2807.
- [54] D. Hoebbel, M. Nacken, H. Schmidt, *J. Sol-Gel Sci. Technol.* 12 (1998) 169.
- [55] I.R. Peterson, G. Brezesinski, B. Struth, E. Scalas, *J. Phys. Chem., B* 102 (1998) 9437.
- [56] M.K. Durbin, A. Malik, A.G. Richter, C.J. Yu, R. Eisenhower, P. Dutta, *Langmuir* 14 (1998) 899.
- [57] J. Harada, K. Ogawa, S. Tomoda, *Acta Crystallogr. B* 53 (1997) 662.